PONTIFICIA UNIVERSIDAD CATÓLICA DEL PERÚ

FACULTAD DE CIENCIAS E INGENIERÍA

BÚSQUEDA DE NEUTRINOS PESADOS VIA FOTONES FUERA DE TIEMPO EN COLISIONADORES

Tesis para obtener el título profesional de Licenciado en Física

AUTOR

Cesar Franco Delgado Dador

ASESOR

Joel Jones Pérez

Lima, Noviembre, 2022

Declaración jurada de autenticidad

Yo, Joel Jones Pérez, docente de la Facultad de Ciencias e Ingeniería de la Pontificia Universidad Católica del Perú, asesor de la tesis/el trabajo de investigación titulado "Búsqueda de neutrinos pesados via fotones fuera de tiempo en colisionadores", del autor César Franco Delgado Dador, dejo constancia de lo siguiente:

- El mencionado documento tiene un índice de puntuación de similitud de 14%. Así lo consigna el reporte de similitud emitido por el software *Turnitin* el 04/11/2022.

- He revisado con detalle dicho reporte y confirmo que cada una de las coincidencias detectadas no constituyen plagio alguno.

- Las citas a otros autores y sus respectivas referencias cumplen con las pautas académicas.

Lugar y fecha: Lima, 23 de noviembre del 2022

Apellidos y nombres del asesor: Jones Pérez, Joel	
DNI: 40711425	Firma
ORCID: 0000-0002-2037-6369	

Resumen

El Modelo Estándar de Física de Partículas (ME) es una teoría que une tres de las interacciones fundamentales de la naturaleza en una solución elegante. Describe las propiedades e interacciones de fermiones con spin ½ y bosones con spin entero. Estos fermiones luego son subdivididos en quarks y leptones. En el ME, los neutrinos se consideran partículas sin masa pero esta característica luego fue refutada por experimentos de oscilación, demostrando que tienen masas de hasta 0.1ev. Esto significa que el ME debe ser extendido para brindar masas a los neutrinos. El mecanismo Seesaw es una de esas extensiones que permite a los neutrinos tener masas mediante la introducción de neutrinos masivos estériles y de mano derecha.

En este trabajo extendemos el modelo Seesaw al añadir operadores efectivos de dimensión 5 que median la producción y decaimiento de neutrinos pesados de larga vida N con masas en el orden de los GeV. Exploramos la producción de N mediante decaimientos exóticos del Higgs a través del operador efectivo neutrino-Higgs. El neutrino pesado luego decae a un neutrino del ME y un fotón por medio del operador dipolar, cuyo decaimiento parcial es calculado de forma analítica. Consideramos dos procesos de producción del Higgs: gluon fusion (GF) y vector boson fusion (VBF). Evaluamos la posible de detección de N con búsquedas de fotones desplazados en el detector ATLAS para energía de colisión de 13 TeV, simulado en MadGraph. Estas búsquedas usaron variables de tiempo retardado e indirección, t_γ y $|\Delta z_\gamma|$, respectivamente. Encontramos que para procesos de GF y VBF, la mayoría de eventos tipo señal pertenecen a las regiones de background y control en lugar de la región de señal, significando que la búsqueda realizada en este trabajo no es sensible al modelo.

Abstract

The Standard Model of Particle Physics (SM) is a theory that unites three of the fundamental interactions of nature into an elegant solution. It describes the properties and interactions of spin ½ fermions and integer spin bosons. These fermions are further divided into quarks and leptons. In the SM, neutrinos are considered massless particles but this characteristic was later disproved by oscillation experiments, showing they carry masses of up to 0.1eV. This means that the SM must be extended in order to provide masses to neutrinos. The Seesaw Mechanism is such an extension, allowing neutrino masses by introducing sterile, right handed, massive neutrinos.

In this work we extend the Seesaw model by adding dimension 5 effective operators, which mediate the production and decay of long-lived heavy neutrinos N with masses in the GeV scale. We explore N production through exotic Higgs decays by way of a neutrino-Higgs effective operator. The heavy neutrino then decays into a SM neutrino and a photon via a dipole operator, whose partial width is calculated analytically. We considered two Higgs production processes: gluon fusion (GF) and vector boson fusion (VBF). We evaluate the possible detection of N through displaced photon searches in the ATLAS detector for 13 TeV collision energy, simulated in MadGraph. These searches employed time-delay and non-pointing variables, t_γ and $|\Delta z_\gamma|$, respectively. We found that for both GF and VBF processes most signal events belong to the background and control regions rather than the signal region, implying the search developed in this work is not sensitive to the model at hand.

Acknowledgement

Contents

List of Tables

List of Figures

1   Introduction

The Standard Model of Particle Physics (SM) is perhaps the most successful scientific theory. It compiles three of the fundamental interactions of nature into a simple, elegant framework. Furthermore, it provides a plethora of experimentally confirmed predictions, strengthening the robustness of the theory. The particle content of the SM is divided in spin 1/2 fermions, and integer spin bosons. The fermions include quarks (u, d, c, s, b, t) and leptons (e^-, μ^-, τ^-, ν_e, ν_μ, ν_τ), as well as their anti particles. The bosons include the spin 1 gauge bosons, or force-carrier particles, for electromagnetic (γ), weak ($W^\pm$, Z), and strong interactions (g), as well as the spin 0 Higgs boson (H).

Neutrinos are leptons of the SM which only carry weak charge, meaning they interact exclusively via the massive weak gauge bosons. At energies below the W mass, these interactions are highly supressed. In the SM, neutrinos are considered to be massless particles due to the fact that only a left-chiral ν_L component is observed in nature, which does not allow to generate a mass term from the Higgs mech-

anism. However, a large series of experimental results starting from Superkamiokande (1998) [1] and lately the KATRIN experiment [2], have shown the neutrinos could have masses of up to $\mathcal{O}(0.8\,\text{eV})$, in partial disagreement with what was proposed by the SM.

Extending the SM with right handed neutrinos ν_R and providing a Yukawa coupling Y_ν is enoguh for generating neutrino masses via Higgs mechanism, however it does not satisfy naturalness. This is because Y_ν would have to be many orders of magnitude smaller than the coupling Y_e of the electron, the next lightest SM particle .

This motivates other extensions of the SM which can explain the small neutrino masses in a more *satisfying* way. One of such extensions is the Seesaw Mechanism [3–6], which extends the SM with sterile, right handed, massive neutrinos N_R. In the simplest realization of the Seesaw Mechanism, the masses of the SM neutrinos ν are inversely proportional to the masses of these heavy neutrinos N (see Chapter 2). Therefore, one may obtain the negligible ν masses by considering very large masses for N (hence the name *seesaw*). If the heavy neutrinos are light enough, they could be produced in

present and near future colliders at TeV collision energies. Further-more, since they share characteristics with light neutrinos like negligible interactions, if they have masses in the GeV scale, one would expect them to have considerable lifetimes in comparison with neutrino scale mass in the eV scale. In this work we consider such Long Lived Heavy neutrinos, and their possible collider phenomenolgy.

It has been shown in previous works [7, 8] that the phenomenology of the Seesaw at the LHC is heavily constrained. To account for this, it is interesting to consider Effective Operators to obtain a richer phenomenology to work with. In this thesis work we explore the collider phenomenology of Long-Lived heavy neutrinos by considering a dipole operator between the Weak gauge boson and the light and heavy neutrinos $B\nu N$, as well as Higgs portal operator with 2 heavy neutrinos $HHNN$. This work is divided as follows: In Chapter 2 we present an extensive Theoretical Review. In Chapter 3 we consider production via the decays of the Higgs and the Dipole operator to mediate the decay of N. Finally in Chapter 4 we conclude.

2 Theoretical Framework

The presence of unsolved questions in particle physics like the neutrino mass problem, might suggest the need to either expand the particle content or add new operators to the SM. For example, to provide masses to neutrinos, one could include the non-renormalizable Weinberg operator,

$$\Delta \mathscr{L} = -\frac{\kappa}{2\Lambda}\bar{L}\tilde{H}\tilde{H}^T L^c + h.c.$$
$$\tilde{H} = i\sigma_2 H^*$$

(1)

which is the only dim-5 operator allowed by the symmetries of the SM. Here L represents the left-handed lepton doublets and H is the Higgs doublet, Λ the scale of new physics, σ_2 a Pauli matrix and κ a model dependent coefficient. After Spontaneous Symmetry Breaking, the Weinberg operator provides a mass term for the neutrinos, which is missing in the SM, as well as cubic and quartic interactions between neutrinos and the Higgs boson. This is of particular relevance, since non zero neutrino masses have been shown to exist after the conception of the SM. However, a theory is considered to lose its

predictivity when one adds non-renormizable operators. Thus, one would hope this operator to arise from a renormalizable and complete model, making it an enticing candidate for physics Beyond the Standard Model (BSM).

2.1 Seesaw Mechanism

Perhaps the simplest and most popular renormalizable theory that reproduces the Weinberg operator (Fig. 1), is the Type I Seesaw Mechanism [3–6]. The SM is extended by n right handed neutrinos N_R, which are singlets under the known gauge symmetries. Therefore, they are also refered to as sterile neutrinos, or heavy neutral leptons.
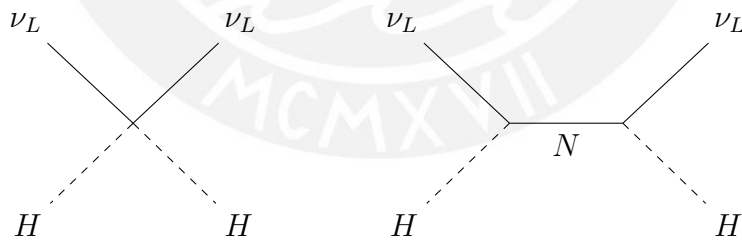

Figure 1: Right: Weinberg Operator. Left: Renormalizable realization via Type I Seesaw Mechanism.

This gauge invariance allows for an explicit mass term, and the SM Lagrangian is appropriately modified by:

$$\Delta \mathcal{L} = -Y_\nu^{ai} \bar{L}_a N_{Ri} \tilde{H} - \frac{\mathbf{M}_{Rij}}{2} \bar{N}_{Ri} N_{Rj}^c + h.c. \qquad (2)$$

where, Y_ν^{ai} are Yukawa couplings with $a = e, \mu, \tau$ and $i, j = s_1, s_2...s_n$ (sterile "flavours"), and $\mathbf{M}_{Rij}$ is the symmetric right handed neutrino Majorana mass matrix.

For a fermion ψ, its charge conjugate is defined by $\psi^C \equiv C\bar{\psi}^T$, where C is the Charge conjugation matrix. A fermion is said to be Majorana if:

$$\psi = \psi^c \qquad (3)$$

That is, a Majorana fermion is equal to its charge conjugate. The charge conjugate of N_R, N_R^c constitutes a left-handed fermion, which allows us to define the left handed $\Psi_L = (\nu_L \; N_R^c)^T$. Here, ν_L contains the three known left handed fermions, while N_R accomodates n new right handed fermions.

After electroweak symmetry breaking, the Lagrangian can be written as:

$$\Delta \mathscr{L} = -\frac{1}{2}\bar{\Psi}_L^c \mathscr{M}_\nu \Psi_L - \frac{1}{2}\bar{\Psi}_L \mathscr{M}_\nu^* \Psi_L^c \tag{4}$$

With $\mathscr{M}_\nu$ as

$$\mathscr{M}_\nu = \begin{pmatrix} 0 & \mathbf{m}_D \\ \mathbf{m}_D^T & \mathbf{M}_R \end{pmatrix} \tag{5}$$

where $\mathbf{m}_D = \frac{v}{\sqrt{2}}Y_\nu^*$ comes from the Yukawa term. A non-diagonal mass matrix will have eigenvalues and eigenvectors that constitute the neutrino mass basis, different from the chirality (or interaction) basis.

We can picture the seesaw mechanism better in a simplified scenario with a single pair of neutrinos, ν_L and N_R. We will denote the mass basis states as ν and N, the light and heavy states, respectively.

As before we have $\Psi_L = (\nu_L \ N_R^c)^T$ with mass matrix:

$$\mathscr{M}_\nu = \begin{pmatrix} 0 & m_D \\ m_D & M_R \end{pmatrix} \tag{6}$$

Here, the Dirac and Majorana mass terms are single values instead

of matrices, and m_D is given by $v\dfrac{Y_\nu^*}{\sqrt{2}}$. In the mass basis $(\nu\; N)$, $\mathscr{M}_\nu$ is given by:

$$\tilde{\mathscr{M}}_\nu = \begin{pmatrix} m_\nu & 0 \\ 0 & M_N \end{pmatrix} \tag{7}$$

We can solve for m_ν and M_N, and assuming $m_D << M_R$:

$$m_\nu \simeq \frac{-m_D{}^2}{M_R}$$
$$M_N \simeq M_R + \frac{m_D{}^2}{M_R} \tag{8}$$

The mass matrix involves Ψ_L and Ψ_L^c in the same way, therefore the mass eigenvectors must correspond to Majorana states. These take the form:

$$\nu \simeq (\nu_L + \nu_L{}^c) - \frac{m_D}{M_R}(N_R + N_R{}^c)$$
$$N \simeq (N_R + N_R{}^c) + \frac{m_D}{M_R}(\nu_L + \nu_L{}^c) \tag{9}$$

which is explicitly invariant under charge conjugation. The light neutrino is mostly active, while the heavy neutrino is mostly sterile. The ratio between the Dirac and Majorana mass terms can be

expressed in terms of the "observable" neutrino masses as $\dfrac{m_D}{m_R} \simeq \sqrt{\dfrac{m_\nu}{M_N}}$. This determines how left and right chiral states mix, and it is expected to be considerably small since it involves a factor of a light neutrino mass divided by a heavy neutrino mass. Since m_ν has to remain around the eV range, this puts very strong constraints on Y_ν and M_R, excluding the possibility of observing such simple scenarios.

2.2 The Low Scale Seesaw

For the purpose of this work we consider 3+3 (n=3) type I Seesaw. As we will see, introducing more right handed neutrinos to the seesaw model increases the number of available parameters. This in turn, allows us to avoid the restrictive relations between neutrino masses and mixing. In particular, we focus on a scenario with two nearly degenerate right-handed massive neutrinos, N_5 and N_6, with masses of $\mathcal{O}\left(\text{GeV}\right)$ and enhanced mixing with active states, and a third arbitrary mass neutrino N_4 with negligible mixing to the other

states [9]. The mass degeneracy is required in order to avoid neutrinoless double beta decay constraints. This scenario will behave like an effective $3 + 2$ model [10], as the third heavy neutrino N_4 will be decoupled from the collider phenomenology.

The parametrization used here is similar to the Casas-Ibarra parameterization [11]. Eq. (5) can be diagonalized by a unitary matrix U; in the flavor basis (where Y_e is diagonal), we have:

$$\mathscr{M}_\nu = U^* \mathscr{M}_\nu^{diag} U^\dagger \tag{10}$$

where the diagonalized mass matrix takes the form:

$$\mathscr{M}_\nu^{diag} = diag(m_1, m_2, m_3, M_4, M_5, M_6) \tag{11}$$

The fermion multiplet in the diagonal (mass) basis is given by $\Psi'_L = U^\dagger \Psi_L$, and finally the Lagrangian is:

$$\Delta\mathscr{L} = -\frac{1}{2}\overline{\Psi'^c_L}\mathscr{M}_\nu^{diag}\Psi'_L - \frac{1}{2}\overline{\Psi'_L}\mathscr{M}_\nu^{diag}\Psi'^c_L \tag{12}$$

This leads again to a Majorana construction for the mass basis fermions:

$$\Psi = \Psi'_L + \Psi'^c_L \tag{13}$$

In Eq. 10, U is the 6×6 analogue to the PMNS matrix. We can decompose it into 3×3 blocks:

$$U = \begin{pmatrix} U_{al} & U_{ah} \\ U_{sl} & U_{sh} \end{pmatrix} \tag{14}$$

where from left to right, top to bottom, each block refers to the active-light, active-heavy, sterile-light and sterile-heavy mixings respectively. Each block can be parameterized as [9, 12]:

$$U_{al} = U_{PMNS}H, \qquad\qquad U_{ah} = iU_{PMNS}Hm_l^{1/2}R^{\dagger}M_h^{-1/2},$$

$$U_{sl} = i\bar{H}M_h^{-1/2}Rm_l^{1/2}, \qquad\qquad U_{sh} = \bar{H} \tag{15}$$

with,

$$H = (I + m_l^{1/2}R^{\dagger}M_h^{-1}Rm_l^{1/2})^{-1/2}$$

$$\bar{H} = (I + M_h^{-1/2}Rm_lR^{\dagger}M_h^{-1/2})^{-1/2} \tag{16}$$

The diagonal heavy neutrino matrix $M_h = diag(M_4, M_5, M_6)$ is a free parameter of the theory. The diagonal light neutrino matrix is denoted by $m_l = diag(m_1, m_2, m_3) = diag(m_1, \sqrt{\Delta m^2_{sol} + m^2_1}, \sqrt{\Delta m^2_{atm} + m^2_1})$, with $m_1 \lesssim 0.8$ eV constrained by the Katrin experiment [2], and Δm^2_{sol} and Δm^2_{atm} the observed light neutrino mass squared differences, by solar and atmospheric neutrino experiments, respectively.

The matrix R is a complex orthogonal matrix, parameterized as:

$$R = \begin{pmatrix} c_{45} & s_{45} & 0 \\ -s_{45} & c_{45} & 0 \\ 0 & 0 & 1 \end{pmatrix} \begin{pmatrix} c_{46} & 0 & s_{46} \\ 0 & 1 & 0 \\ -s_{46} & 0 & c_{46} \end{pmatrix} \begin{pmatrix} 1 & 0 & 0 \\ 0 & c_{56} & s_{56} \\ 0 & -s_{56} & c_{56} \end{pmatrix} \quad (17)$$

where s_{ij} and c_{ij} are the sines and cosines of three complex angles, $\theta_{ij} + i\gamma_{ij}$. Along with the 2 Majorana CP phases of U_{PMNS}, and $\mathbf{M}_H$ these are the 11 free parameters of the theory. For this study we take interest in the case where only one γ_{ij} (in this case γ_{56}) is different from 0 and considerably large ($|\gamma_{ij}| \gtrsim 1$). Here N_4 becomes decoupled as mentioned before, and R can be written as:

$$R_{56}(\theta_{56}, \gamma_{56}) = \begin{pmatrix} 1 & 0 & 0 \\ 0 & c_{56} & s_{56} \\ 0 & -s_{56} & c_{56} \end{pmatrix} \tag{18}$$

We expand the trigonometric functions as:

$$\cos(\theta_{56} + i\gamma_{56}) = \cos(\theta_{56})\cosh(\gamma_{56}) - i\sin(\theta_{56})\sinh(\gamma_{56})$$
$$\sin(\theta_{56} + i\gamma_{56}) = \sin(\theta_{56})\cosh(\gamma_{56}) + i\cos(\theta_{56})\sinh(\gamma_{56}) \tag{19}$$

For large γ_{56} we have $\sinh(\gamma_{56}) \approx z_{56}\cosh(\gamma_{56})$, where z_{56} is the sign of γ_{56}. Then we can rewrite eq. (19) as:

$$\cos(\theta_{56} + i\gamma_{56}) = \cosh(\gamma_{56})\left(\cos(\theta_{56}) - iz_{56}\sin(\theta_{56})\right) = \cosh(\gamma_{56})e^{-iz_{56}\theta_{56}}$$
$$\sin(\theta_{56} + i\gamma_{56}) = \cosh(\gamma_{56})\left(\sin(\theta_{56}) + iz_{56}\cos(\theta_{56})\right) = iz_{56}\cosh(\gamma_{56})e^{-iz_{56}\theta_{56}}$$
$$\tag{20}$$

Now we can rewrite R and we see that θ_{56} behaves like an overall

phase:

$$R_{56}(\theta_{56}, |\gamma_{56}| >> 0) = \begin{pmatrix} 1 & 0 & 0 \\ 0 & \cosh(\gamma_{56})e^{-iz_{56}\theta_{56}} & iz_{56}\cosh(\gamma_{56})e^{-iz_{56}\theta_{56}} \\ 0 & -iz_{56}\cosh(\gamma_{56})e^{-iz_{56}\theta_{56}} & \cosh(\gamma_{56})e^{-iz_{56}\theta_{56}} \end{pmatrix}$$

$$(21)$$

Assuming $H \sim I$, we can write the active to heavy elements of U_{ah} as:

$$U_{a4} = (U_{PMNS})_{a1}\sqrt{\frac{m_1}{M_4}} \tag{22}$$

$$U_{a5} = -iz_{56}Z_a\sqrt{\frac{m_3}{M_5}}\cosh(\gamma_{56})e^{iz_{56}\theta_{56}} \tag{23}$$

$$U_{a6} = Z_a\sqrt{\frac{m_3}{M_6}}\cosh(\gamma_{56})e^{iz_{56}\theta_{56}} \tag{24}$$

with:

$$Z_a = (U_{PMNS})_{a3} + iz_{56}\sqrt{\frac{m_2}{m_3}}(U_{PMNS})_{a2} \tag{25}$$

The term $|U_{\mu4}|^2$ receives no enhancement from $\cosh(\gamma_{56})$, and

depends only on U_{PMNS} and the ratio of light and heavy neutrino masses. On the other hand, both U_{a5} and U_{a6} can be greatly enhanced by $\cosh{(\gamma_{56})}$. We analyze a section of the parameter space defined by the following conditions:

$$m_1 = 10^{-2} \text{ eV}$$

$$M_4 = 1 \text{ MeV}$$

$$15 \text{ GeV} < M_5 \approx M_6 < 50 \text{ GeV} \qquad (26)$$

$$\gamma_{46} = \gamma_{45} = 0$$

$$5 < |\gamma_{56}| < 10$$

Heavy neutrinos interact via the weak gauge bosons due to their mixing with the active states. In this simple scenario N_5 and N_6 decay $\sim 100\%$ to three fermions, and the individual branching ratios depend mainly on color and kinematic factors. The mixing dependence vanishes because of a cancellation between partial and total decay widths. For this choice of parameters, we adjust γ_{56} accordingly to allow N_5 and N_6 to have a long-lived particle behaviour with decay lengths between $10^{-3}m$ and $1m$ as seen in Fig. 2.
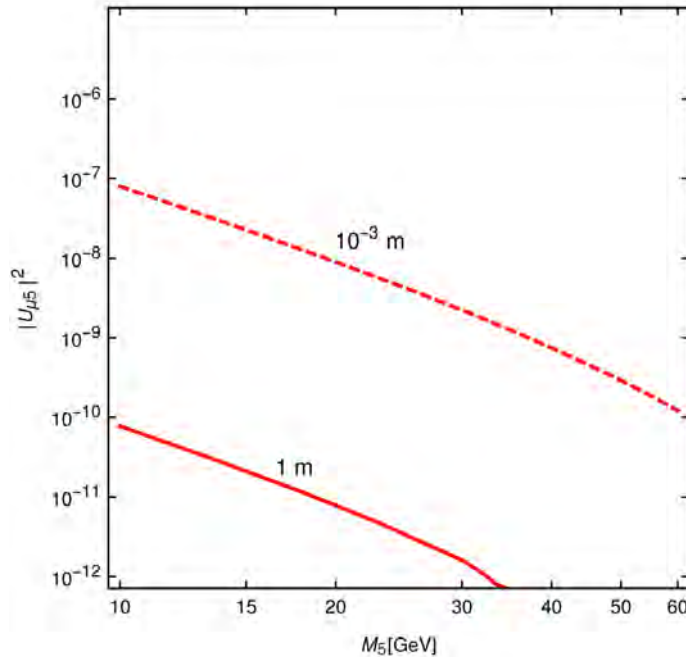
Figure 2: Decay length for $M_5 \approx M_6$. The solid red line corresponds to a decay length of 1 meter. The dashed red line for 1 millimeter.

This zone of the parameter space is testable with existing experiments, in particular the LHC, and the near-future HL-LHC. The model was implemented in SARAH [13], and the decay widths were calculated in SPheno [14, 15] (see Appendix A).

2.3 Neutrino-Higgs Effective Operator

The addition of N_R allows for a larger variety of Gauge invariant dimension five Effective Operators. One such operator describes the interaction between two right handed neutrinos and two Higgs dou-

blets [16, 17]:

$$\Delta\mathcal{L} = \frac{\lambda_{st}}{\Lambda}\, \bar{N}^c_{R_s}\, N_{R_t}\, H^\dagger\, H + \text{h.c.} \tag{27}$$

After electroweak symmetry breaking, this operator can greatly enhance the decay of the Higgs into two heavy neutrinos, provided that $2m_{N_R} < m_h$. The effective Lagrangian for the 3-point vertex is then given by:

$$\mathcal{L} = (\alpha_{NH})_{st}\, \bar{N}^c_{R_s}\, N_{R_t}\, h + \text{h.c.} \tag{28}$$

where $(\alpha_{NH})_{st} \equiv \lambda_{st}\, v_{\text{SM}}/\Lambda$.

We can perform a rotation into the mass basis, taking into consideration the Majorana construction of the states. For the heavy neutrinos this yields:

$$\mathcal{L} = (\alpha'_{NH})_{ij}\, \bar{N}_i P_L\, N_j\, h\, +\, (\alpha'^*_{NH})_{ij}\, \bar{N}_i P_R\, N_j\, h \tag{29}$$

where $(\alpha'_{NH})_{ij} = U_{ai}(\alpha_{NH})_{ab}\, U_{bj}$

Taking $(\alpha'_{NH})_{ij}$ real and $(\alpha'_{NH})_{55} = \alpha_h$, with all other entries equal to 0, this reduces to:

17

$$\mathcal{L}_{hNN} = \alpha_h \, \bar{N}_5 \, N_5 \, h \qquad (30)$$

This term also arises from the Weinberg operator in eq. (1), but it is greatly suppressed by the active to heavy neutrino mixing U_{a5}. As we will see, we are very interested in Higgs mediated neutrino production, so eq. (30) will allow us to enhance the heavy neutrino production cross section, without affecting other aspects of the phenomenology.

2.4 Neutrino dipole effective operator

Another possibility is the dimension 5 neutrino dipole operator [18]:

$$\Delta\mathcal{L} = \frac{(\alpha_{NB})_{st}}{\Lambda} \, \bar{N}^c_{R_s} \, B_{\mu\nu} \sigma^{\mu\nu} N_{R_t} + \text{h.c.} \qquad (31)$$

Following similar steps as above, and considering only the interaction between light and heavy states, this simplifies to [19]:

$$\mathcal{L} = d_\gamma \bar{\nu}_l F_{\mu\nu} \sigma^{\mu\nu} N + \text{h.c.} \qquad (32)$$

for a single family of light leptons $d_\gamma \equiv c_W U_{is} \dfrac{(\alpha_{NB})_{st}}{\Lambda} U_{t4}$, where c_W comes from the relation between $B_{\mu\nu}$ and $F_{\mu\nu}$ (the electromagnetic field strength tensor), and i can go from 1 to 3. Here N represents a singlet fermionic state and ν_l is a SM l-neutrino field. There is also a term describing the interaction of neutrinos and $Z_{\mu\nu}$, which has not been considered for the phenomenology described in this work.

This generates a seemingly anomalous interaction between photons and neutrinos. Expanding the electromagnetic tensor, we have

$$i\mathcal{L} = d_\gamma \bar{\nu}_l (\partial_\mu A_\nu - \partial_\nu A_\mu)\sigma^{\mu\nu} N \tag{33}$$

After multiplying the terms, this yields

$$i\mathcal{L} = d_\gamma \bar{\nu}_l (\partial_\mu A_\nu \sigma^{\mu\nu} + \partial_\nu A_\mu \sigma^{\nu\mu}) N$$

where we have used the property $\sigma^{\mu\nu} = -\sigma^{\nu\mu}$. We see that both terms in the parenthesis are the same. Going to momentum space $i\partial_\mu \to p_\mu^{(\gamma)}$, where $p_\mu^{(\gamma)}$ is the photon's momentum; we now have:

$$\mathcal{L}_{\gamma N \nu_l} = -2i d_\gamma \bar{\nu}_l p_\mu^{(\gamma)} A_\nu \sigma^{\mu\nu} N + \text{h.c.} \tag{34}$$

In this work, we are interested in $N \to \gamma\nu$, namely the decay of a heavy neutrino N into a photon and a SM neutrino, process enabled by the dipole portal described above. This phenomenology allows us to use photon and missing energy searches in order to test for constrains on d_γ.

In the following, we will calculate the decay width for the process in mention. From Eq. 34, our vertex factor is: $-2id_\gamma p_\mu^{(\gamma)} \sigma^{\mu\nu} P_R$. Following the usual rules of Feynman Calculus, we add the factors corresponding to in and out-going states in order to compute the process amplitude:

$$\mathcal{M} = 4d_\gamma \bar{u}(\nu) p_\mu^{(\gamma)} \sigma^{\mu\nu} P_R u(N) \epsilon_\nu^* \qquad (35)$$

where we have omitted the subscript l from ν_l to avoid an excess of indices later in the calculation. Then,

$$|\mathcal{M}|^2 = 16|d_\gamma|^2 \left[\bar{u}(\nu) p_\mu^{(\gamma)} \sigma^{\mu\nu} P_R u(N) \epsilon_\nu^* \right] \left[\epsilon_\beta^T u(N)^\dagger P_R \left(\sigma^{\alpha\beta} \right)^\dagger p_\alpha^{(\gamma)} \gamma^0 u(\nu) \right]$$

$$(36)$$

Summing over all possible helicities and polarizations, we get:

$$\sum_{\nu,N,\gamma} |\mathcal{M}|^2 = -16|d_\gamma|^2 Tr \left[P_R p_\mu^{(\gamma)} \sigma^{\mu\nu} \left(\not{p}^{(N)} + m_N \right) g_{\nu\beta} P_L \sigma^{\alpha\beta} p_\alpha^{(\gamma)} \left(\not{p}^{(\nu)} \right) \right]$$

$$= -16|d_\gamma|^2 p_\mu^{(\gamma)} p_\lambda^{(N)} p_\alpha^{(\gamma)} p_\epsilon^{(\nu)} Tr \left[P_R \sigma^{\mu\nu} \gamma^\lambda g_{\nu\beta} \sigma^{\alpha\beta} \gamma^\epsilon \right] \qquad (37)$$

where we have used Casimir's trick to find $u(N)\bar{u}(N)$, and where $p^{(N)}$ is the heavy neutrino's momentum. The trace term can be expressed as the sum of two separate traces:

$$Tr \left[P_R \sigma^{\mu\nu} \gamma^\lambda g_{\nu\beta} \sigma^{\alpha\beta} \gamma^\epsilon \right] = \frac{1}{2} Tr \left[\sigma^{\mu\nu} \gamma^\lambda \sigma_\nu^\alpha \gamma^\epsilon \right] + \frac{1}{2} Tr \left[\gamma^5 \sigma^{\mu\nu} \gamma^\lambda \sigma_\nu^\alpha \gamma^\epsilon \right]$$
$$(38)$$

where we have used $g_{\nu\beta} \sigma^{\alpha\beta} = \sigma_\nu^\alpha = \frac{i}{2}(\gamma^\alpha \gamma_\nu - \gamma_\nu \gamma^\alpha)$. Lets focus on the first trace. After expanding the sigma matrices, we can express it as the sum of 4 different traces:

$$-\frac{1}{4} Tr \left[\gamma^\mu \gamma^\nu \gamma^\lambda \gamma^\alpha \gamma_\nu \gamma^\epsilon \right] = -g^{\lambda\alpha} Tr \left[\gamma^\mu \gamma^\epsilon \right]$$

$$\frac{1}{4} Tr \left[\gamma^\nu \gamma^\mu \gamma^\lambda \gamma^\alpha \gamma_\nu \gamma^\epsilon \right] = -\frac{1}{2} Tr \left[\gamma^\alpha \gamma^\lambda \gamma^\mu \gamma^\epsilon \right] \qquad (39)$$

$$\frac{1}{4} Tr \left[\gamma^\mu \gamma^\nu \gamma^\lambda \gamma_\nu \gamma^\alpha \gamma^\epsilon \right] = -\frac{1}{2} Tr \left[\gamma^\mu \gamma^\lambda \gamma^\alpha \gamma^\epsilon \right]$$

$$-\frac{1}{4} Tr \left[\gamma^\nu \gamma^\mu \gamma^\lambda \gamma_\nu \gamma^\alpha \gamma^\epsilon \right] = -g^{\mu\lambda} Tr \left[\gamma^\alpha \gamma^\epsilon \right]$$

Solving these using the well known properties for the trace on gamma matrices we get our expression for the first trace in Eq. 38 as:

$$Tr\left[\sigma^{\mu\nu}\gamma^\lambda\sigma_\beta^\alpha\gamma^\epsilon\right] = -8g^{\mu\lambda}g^{\alpha\epsilon} - 8g^{\mu\epsilon}g^{\lambda\alpha} + 4g^{\mu\alpha}g^{\lambda\epsilon} \qquad (40)$$

The second trace in Eq. 38 is expanded to the same terms as those in Eq. 39 but with an added γ^5 before the other gamma matrices. These traces are well known, for instance, $Tr\left[\gamma^5\gamma^\mu\gamma^\nu\right] = 0$, which only leaves us with the middle terms. Hence:

$$Tr\left[\gamma^5\sigma^{\mu\nu}\gamma^\lambda\sigma_\beta^\alpha\gamma^\epsilon\right] = -2i\epsilon^{\alpha\lambda\mu\epsilon} - 2i\epsilon^{\mu\lambda\alpha\epsilon} = 0 \qquad (41)$$

Here, the second Levi-Civita symbol is an odd permutation to the first one ($\epsilon^{\mu\lambda\alpha\epsilon} = -\epsilon^{\alpha\lambda\mu\epsilon}$). Finally, Eq. 38 becomes

$$Tr\left[P_R\sigma^{\mu\nu}\gamma^\lambda g_{\nu\beta}\sigma^{\alpha\beta}\gamma^\epsilon\right] = -4g^{\mu\lambda}g^{\alpha\epsilon} - 4g^{\mu\epsilon}g^{\lambda\alpha} + 2g^{\mu\alpha}g^{\lambda\epsilon}$$

$$(42)$$

Replacing this result in our amplitude and denoting $\sum_{\nu,N,\gamma}|\mathcal{M}|^2$ simply as $|\mathcal{M}|^2$, we get

$$|\mathcal{M}|^2 = 16|d_\gamma|^2 p_\mu^{(\gamma)} p_\lambda^{(N)} p_\alpha^{(\gamma)} p_\epsilon^{(\nu)} \left(4g^{\mu\lambda} g^{\alpha\epsilon} + 4g^{\mu\epsilon} g^{\lambda\alpha} - 2g^{\mu\alpha} g^{\lambda\epsilon} \right)$$

$$= 64|d_\gamma|^2 \left[2 \left(p^{(\gamma)} \cdot p^{(N)} \right) \left(p^{(\gamma)} \cdot p^{(\nu)} \right) - \frac{1}{2} p^{(\gamma)2} \left(p^{(N)} \cdot p^{(\nu)} \right) \right]$$

The last term in the equation above is zero since $p^{(\gamma)2} = m_\gamma^2 = 0$.

Finally, averaging over the initial states,

$$\langle |\mathcal{M}|^2 \rangle = 128|d_\gamma|^2 \left(p^{(\gamma)} \cdot p^{(N)} \right) \left(p^{(\gamma)} \cdot p^{(\nu)} \right) \tag{43}$$

Solving in the process' center of mass frame (where $\bar{p}_N = 0$),

$$\langle |\mathcal{M}|^2 \rangle = 128|d_\gamma|^2 E_\gamma m_N \left(E_\gamma E_\nu - \bar{p}_\gamma \cdot \bar{p}_\nu \right)$$

Given $m_\gamma = m_\nu = 0$, we now take $|\bar{p}_\gamma| = E_\gamma$ and $|\bar{p}_\nu| = E_\nu$, and denoting θ as the angle between the photon's momentum and the neutrino's momentum, we find:

$$\langle |\mathcal{M}|^2 \rangle = 128|d_\gamma|^2 E_\gamma^2 E_\nu m_N \left(1 - cos\theta \right) \tag{44}$$

Here we set $\theta = \pi$ since we are in the center of mass frame. Due to conservation of four-momentum before and after the decay, we get:

$$p_N^2 = (p_\gamma + p_\nu)^2$$

$$\implies m_N^2 = 2p_\gamma \cdot p_\nu$$

$$= 2\left(E_\gamma E_\nu - \bar{p}_\gamma \cdot \bar{p}_\nu\right)$$

$$\implies \frac{m_N^2}{2} = 2E_\gamma E_\nu \tag{45}$$

Replacing Eq. 45 in Eq. 44 we get the final result for the amplitude,

$$\langle |\mathcal{M}|^2 \rangle = 64|d_\gamma|^2 E_\gamma m_N^3 \tag{46}$$

We replace Eq. 46 in the differential width equation for 2-body decay processes:

$$d\Gamma_{N\to\gamma\nu} = \frac{1}{2m_N} 64|d_\gamma|^2 E_\gamma m_N^3 (2\pi)^4 \frac{\delta^4\left(p^{(N)} - p^{(\gamma)} - p^{(\nu)}\right)}{4(2\pi)^6 E_\gamma E_\nu} d^3\bar{p}_\gamma d^3\bar{p}_\nu$$

$$= \frac{2|d_\gamma|^2 m_N^2}{\pi^2 E_\nu} \delta\left(E_N - E_\gamma - E_\nu\right) \delta^3\left(-\bar{p}_\gamma - \bar{p}_\nu\right) d^3\bar{p}_\gamma d^3\bar{p}_\nu$$

Integrating over $d^3\bar{p}_\nu$ we get $\bar{p}_\gamma = -\bar{p}_\nu$ through the Dirac delta properties. Recalling that $E_{\gamma/\nu} = |\bar{p}_{\gamma/\nu}|$,

$$d\Gamma_{N\to\gamma\nu} = \frac{2|d_\gamma|^2 m_N^2}{\pi^2|\bar{p}_\gamma|}\delta\left(m_N - 2|\bar{p}_\gamma|\right)|\bar{p}_\gamma|^2 d|\bar{p}_\gamma|d\Omega_\gamma \qquad (47)$$

where $d^3\bar{p}_\gamma = |\bar{p}_\gamma|^2 d|\bar{p}_\gamma|d\Omega_\gamma$. Hence,

$$\frac{d\Gamma_{N\to\gamma\nu}}{d\Omega_\gamma} = \frac{|d_\gamma|^2 m_N^3}{\pi^2} \qquad (48)$$

Finally, integrating over the solid angle we get the width for the decay of $N \to \gamma\nu$,

$$\Gamma_{N\to\gamma\nu} = \frac{2|d_\gamma|^2 m_N^3}{\pi} \qquad (49)$$

which in turn can be expressed in terms of $(\alpha'_{NB})_{ij} = U_{si}\left(\alpha_{NB}\right)_{st}U_{tj}$ for each particular heavy neutrino j and SM i-neutrino as:

$$\Gamma_{N_j\to\gamma\nu_i} = 2c_W^2 \frac{m_{N_j}^3}{\pi}\left|\frac{(\alpha'_{NB})_{ij}^2}{\Lambda}\right| \qquad (50)$$

This result is the partial width for the decay of a heavy neutrino into a SM neutrino and a photon via the dipole operator and was implemented in our model. For the parameter space of interest, this decay

channel dominates over the 3 body decays, for $\alpha_{NB} \gtrsim 10^{-5} GeV^{-1}$.

3 Long-Lived Heavy Neutrinos via Higgs decay

In this work we are interested in neutral current production of heavy neutrinos via the Higgs boson, followed by their decay into a photon and a light neutrino. From the perspective of a minimal model, consisting only on the Type I Seesaw, the decay $h \to N\,N$ has negligible branching ratio due to the small "active to heavy" mixing of the U matrix. This means, only decays of the form $h \to \nu\,N$ are available. Furthermore, since the production and decay mechanisms are both mediated by the Seesaw, they are heavily correlated. Since we are interested in long-lived heavy neutrinos, the small mixing required for the large decay length decreases the cross-section considerably.

Instead, we extend our initial model by the effective operator described in Section 2.3 in order to have the Higgs branching ratio to two heavy neutrinos as a free parameter. This is currently constrained

only by the measured $BR(h \to \text{exotic}) \lesssim 21\%$ [20, 21]. We can consider values of the effective coupling $\frac{\alpha_{NH}}{\Lambda}$ up to $\mathcal{O}(10^{-5} GeV^{-1})$ for masses around 50 GeV, without exceeding the constraint [22]. We chose $BR(h \to NN) = 0.15$.

We consider the two main Higgs production mechanisms available at the LHC, namely Vector Boson Fusion (VBF) and Gluon Fusion (GF). In Table 1 we can see the cross section for both processes at the LHC. For GF the production chain is $pp \to H$, $H \to N_j N_j$, $N_j \to \nu_i \gamma$, while for VBF we have $pp \to Hjj$, $H \to N_j N_j$, $N_j \to \nu_i \gamma$. At 13 TeV and $m_H = 125$ GeV these processes have cross section 3.727 pb and 43.62 pb respectively. Despite having a cross section an order of magnitude smaller, the topology of the VBF jets (denoted by j) can be used as a very powerful trigger. Thus, one may have more relaxed cuts on the decay products of N. In contrast to this, for GF one must rely on the decay products in order to trigger. Since both relevant heavy neutrinos have nearly identical properties, we consider without loss of generality that the Higgs decays only to N_5.

Process	Correction Order	Cross-section (pb)	K-factor
GF	NNLO+NNLL QCD & NLO EW	43.62	2.48
	LO (Madgraph)	17.57	
VBF	NNLO QCD & NLO EW	3.727	1.41
	LO (Madgraph)	2.65	

Table 1: Table comparing Madgraph's cross section to CERN's reports [23] for Higgs production processes.

Since MadGraph only considers leading order (LO) contributions for Higgs production, we consider the calculated cross-section results for next-to leading order (NLO) and next-to-next-to leading order (NNLO) from CERN's Yellow Report for GF and VBF production [23]. To factor in NLO contributions in our simulated events, we use the K-factor, which is the ratio between NLO and LO cross-section values. These results are shown in Table 1.

3.1 Event Selection and Triggers

Here we present event triggers and cuts used in searches for heavy neutral long-lived particles decaying into a photon and another neutral, stable particle (in our case, the light neutrino). These cuts come from an 8 TeV and 20.3 fb^{-1} luminosity search for displaced diphotons and missing energy carried out by [24]. Our objective is to extrapolate this search to 13 TeV and 300 fb^{-1}, to naively estimate the

final number of events that could be observed at ATLAS.

We analyze a diphoton + missing energy final state, which is most sensitive to LLP pair-production. The heavy neutrino is required to decay inside the detector, before reaching the calorimeters, otherwise the event is discarded. Following [24], we require 2 final state photons with p_T of at least 50 GeV, where both reach the EM calorimeters at the detector ($|\eta|<2.37$ for ATLAS, excluding $1.37<|\eta|<1.52$, the transition region between the barrel and endcap) as specified in Table 2. At least one photon is required to reach the EM barrel region of $|\eta|<1.37$ since events where both photons reach the endcap region provide almost no contribution to the signal sensitivity.

Event Selection	
# photons	2
$p_T^{lead}(\gamma)$	> 50
$p_T^{sublead}(\gamma)$	> 50
$|\eta_\gamma|$	< 2.37 (excluding $1.37 < |\eta| < 1.52$)

Table 2: Selection criteria for final state photon analysis. At least 1 photon should be in the barrel region $|\eta_\gamma|<1.37$.

The previous triggers apply for both GF and VBF type of events. In the latter, two high p_T forward jets are produced and travel in opposite directions in the detector [25]. In principle, these jets could be

used for triggering a measurement by discarding others with multijet backgrounds. VBF cuts for this work were based in [10], which contains the same process for producing a Higgs Boson later decaying into two LLP's and are described in Table 3 below.

VBF Selection	
$p_T(j1)$	>30 GeV
$|\eta^{(}j_1)|$	< 5.0
$p_T(j2)$	>30 GeV
$|\eta(j2)|$	< 5.0
$\eta(j1) \cdot \eta(j2)$	<0
$|\Delta\eta(j1, j2)|$	>4.2
m_{j1j2}	>750 GeV
$\sum_j p_T$	>200 GeV

Table 3: Selection criteria for VBF where $j1$ and $j2$ correspond to the two most energetic jets.

Noticeably, a large invariant mass m_{j1j2} is required. Also, the last cut represents a sum over all hadronic activity in the event to be analyzed. VBF triggers could be used instead of photon triggers, see [22] for details.

The analysis is done over final state photons resulting from the decay of $N_j \rightarrow \nu_i\gamma$, from which we obtain both non-pointing and delayed photons. Non-pointing photons have flight paths that do not trace back to the primary vertex (PV) of the event. Delayed photons arrive later at the detector's calorimeter than would be expected

if they were produced in the PV. In order to determine -at detector level- which events produce non-pointing photons, we use $|\Delta z_\gamma|$, a variable which represents the separation along the detector's z-axis (beamline direction), between the event's PV (Primary Vertex) and the projected origin of the photon, as shown in Fig. 3.
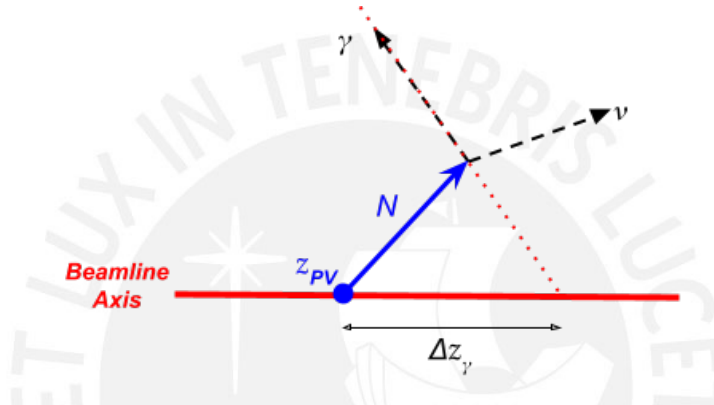

Figure 3: Non-pointing photon vertex reconstruction as it reaches the EM calorimeters. The red-dotted line represents the photon's trajectory projection.

$|\Delta z_\gamma|$ is calculated using:

$$|\Delta z_\gamma| = \left| \frac{r_z - p_z \left(\bar{p} \cdot \bar{r}\right)/|\bar{p}|^2}{1 - p_z^2/|\bar{p}|^2} - z_{PV} \right| \qquad (51)$$

In Eq. 51, $\bar{p}$ is the corresponding photon's momentum and $\bar{r}$ is a point in the photon's trajectory. Also, p_z and r_z are the z-components (along the beamline axis) of $\bar{p}$ and $\bar{r}$ respectively, and z_{PV} the primary vertex' position along the beamline. The derivation of Eq. 51 can be seen in Appendix C.

On the other hand, a photon produced from the decay of a long-lived heavy neutrino inside the detector would take longer to arrive to the calorimeter than a prompt photon would. In order to find these delayed photons we use t_γ, the photon's relative time of arrival at the calorimeter (defining zero as the moment a prompt photon from the hard collision would reach the same position as the delayed photon in the calorimeter, hence $t_\gamma = t_{delayed} - t_{prompt}$).

As described in Section 3.1, at least one of the two photons selected for the analysis must be in the detector's barrel region. In the case where one photon is in the barrel and the second one in the endcap region, the analysis uses the $|\Delta z_\gamma|$ and t_γ values of the barrel photon. In the case where both photons arrive at the EM calorimeter barrel region, the analysis uses the $|\Delta z_\gamma|$ and t_γ measurements of the photon with the highest value for t_γ. This approach avoids the complexity of dealing with the measurements from both photons and their correlation in a single event while providing a similar sensitivity [24].

In [24], event samples are further divided into 4 regions accord-

ing to the measured missing transverse energy $\not{E}_T$, where a high $\not{E}_T$ distinguishes the signal region from the low $\not{E}_T$ prompt background region, as seen in Table 4. Both CR1 and CR2 are used to validate the analysis and background model.

Region	$\not{E}_T$ [GeV]
Signal Region (SR)	>75
Control Region 2 (CR2)	[50, 75]
Control Region 1 (CR1)	[20, 50]
Prompt Background (Bkg)	<20

Table 4: Definition of the different regions on the analysis based on each event's transverse missing energy.

Detector efficiencies were not taken into account in this analysis.

3.2 Results

We have worked with the two Higgs production processes described earlier, generating 10000 events for each via MadGraph (see Appendix A and B). For GF the production chain is $pp \rightarrow H$, $H \rightarrow N_j N_j$, $N_j \rightarrow \nu_i \gamma$, while for VBF we have $pp \rightarrow Hjj$, $H \rightarrow N_j N_j$, $N_j \rightarrow \nu_i \gamma$, with topologies like the ones shown in Fig. 4.

Two masses were considered for the lightest heavy neutrino produced from the Higgs decay, $M_5 = 15$ GeV and $M_5 = 50$ GeV ($M_6 = M_5 + 0.001$ GeV). For each, two squared mixing values were

chosen in order to get either prompt or delayed N decays. For the 15 GeV mass, we chose $|U_{lN}|^2 = 10^{-6}$ (10^{-10}) to get prompt (delayed) decays, while for the 50 GeV mass we chose $|U_{lN}|^2 = 10^{-6}$ (10^{-12}) to get prompt (delayed) decays. The delayed scenario had a decay length of ~ 1m.
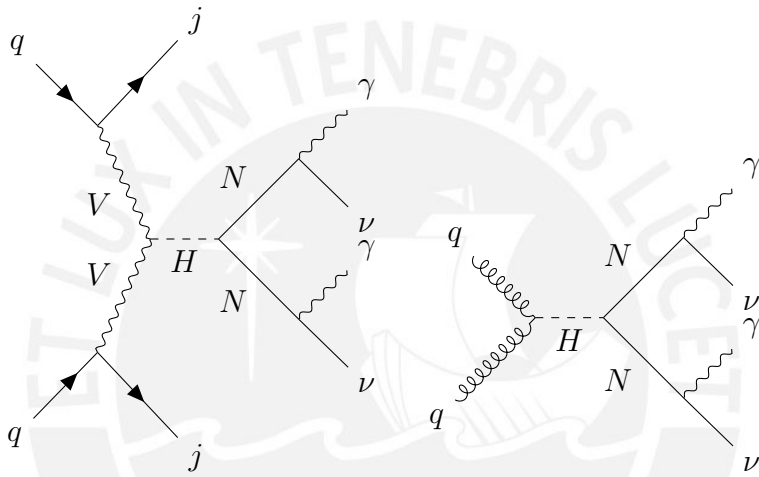

Figure 4: Feynman diagrams for the processes to be analyzed through VBF (left) and GF (right) Higgs production.

The scenarios with prompt heavy neutrinos were used to determine t_{prompt} as a function of pseudorapidity η. This depends only on the geometry of the detector, since prompt photons travel in a straight line at speed of light c from the same origin (PV).

We show in Fig. 5 the different values of the absolute arrival time of the photons, for all considered scenarios. We see that the relative
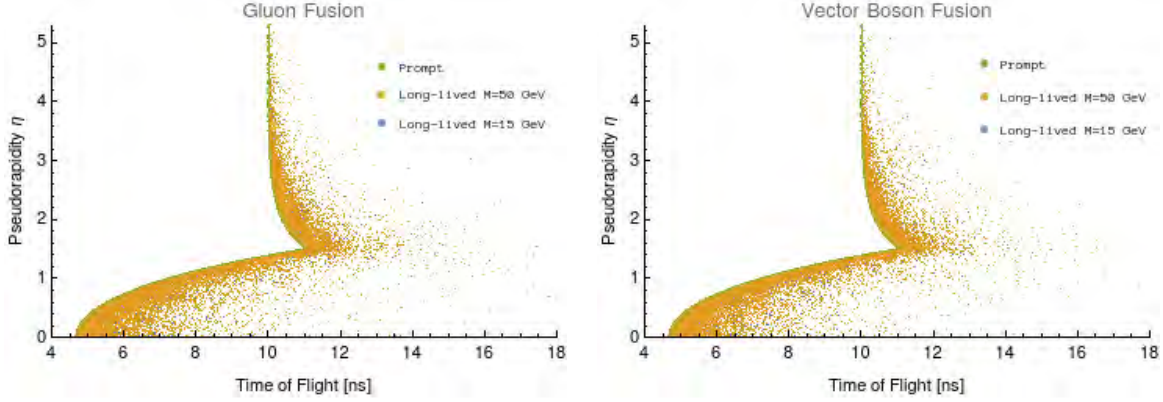
Figure 5: Pseudorapidity of photons arriving at ATLAS EM calorimeters as a function of their time of flight for the chosen scenarios. Green for prompt N, orange and blue for long-lived N, with masses of 50GeV and 15GeV respectively.

t_γ takes values of up to 8ns but in most cases is lower than 2ns.

The distributions for $|\Delta z_\gamma|$ and t_γ are shown in Fig. 6 and Fig. 7 respectively.
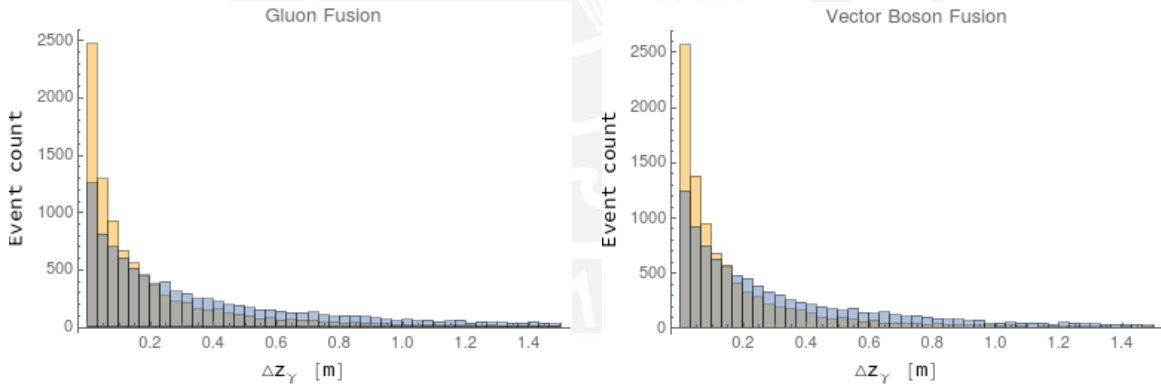

Figure 6: Event distribution for $|\Delta z_\gamma|$ in events with long-lived N. Orange bars for $m_N = 15$ GeV ($|U_{lN}|^2 = 10^{-10}$) and blue for $m_N = 50$ GeV ($|U_{lN}|^2 = 10^{-12}$). Bin width is set at 0.033 m.

Events shown in Fig. 6 and 7 correspond to generated events from the simulation before analysis. We see there is a greater number of events for $m_N = 15GeV$ in all cases. More importantly, there is no
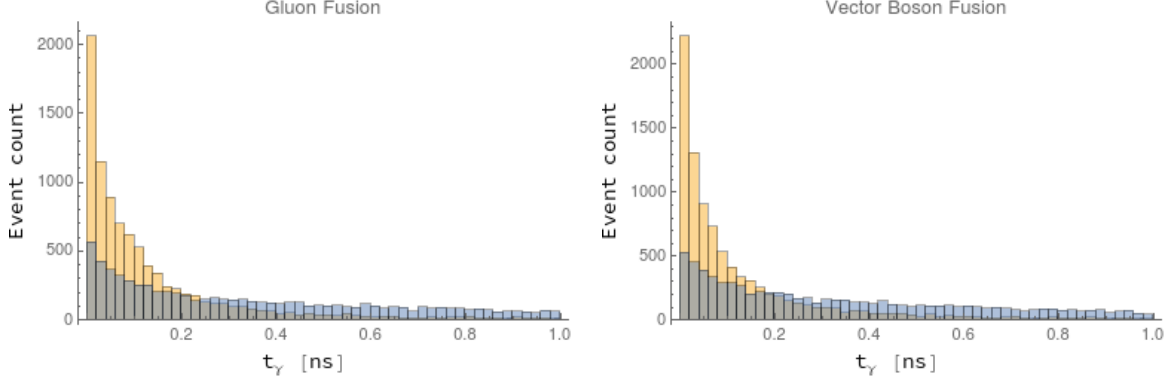
Figure 7: Event distribution for t_γ in events with long-lived N. Orange bars for $m_N = 15$ GeV ($|U_{lN}|^2 = 10^{-10}$) and blue for $m_N = 50$ GeV ($|U_{lN}|^2 = 10^{-12}$). Bin width is set at 0.02 ns.

bigger difference in the distributions between GF and VBF events.

As mentioned earlier, in [24], events are categorized by their $|\Delta z_\gamma|$ measurements into 6 categories, where for each, events are then binned according to t_γ. This method of dividing the events avoids a more data-intensive approach if we were to populate every single bin in a $|\Delta z_\gamma|$ vs. t_γ plot. Instead we use 6 plots (one for each $|\Delta z_\gamma|$ interval) according to the values suggested in Table 5.

Range of $|\Delta z_\gamma|$ values [mm]					
0 - 40	40 - 80	80 - 120	120 - 160	160 - 200	200 - 2000
Bins and range of t_γ values for each bin [ns]					
Bin 1	Bin 2	Bin 3	Bin 4	Bin 5	Bin 6
0 - 0.5	0.5 - 1.1	1.1 - 1.3	1.3 - 1.5	1.5 - 1.8	1.8 - 4.0

Table 5: Values for $|\Delta z_\gamma|$ and t_γ bins.

After the event selection and triggers as discussed in Section 3.1, we find the number of events (NoE) resulting from the analysis, for

each of the regions from Table 4. Then we scale this results to get a corrected "real" number of events after-cuts, taking into account the higgs decay branching ratio $BR(h \rightarrow NN)$, K-factor, MadGraph's cross-section, the number of initial generated events and the LHC's integrated luminosity for the search (L_{LHC}):

$$NoE_{Real} = \frac{NoE_{AfterCuts} * BR(h \rightarrow NN) * K_{factor} * CrossX * L_{LHC}}{NoE_0}$$

(52)

with $NoE_0 = 10000$ and $L_{LHC} = 300 fb^{-1}$. The final "real" values for the analysis described in Table 2 can be seen in Table 6, where for all the regions, Higgs production through GF leaves us with a higher number of events after the cuts compared to VBF. Furthermore, events for decays into N with $m_N = 15 GeV$ are almost an order of magnitude higher than for $m_N = 50 GeV$. It is clear that our model has a large number of events in the SR, Bkg and CR regions.

In [24], Table V shows 386 as the number of background events in the signal region. By doing a simple exercise we can naively extrapolate this value for a luminosity of 300 fb^{-1} (from 20.3 fb^{-1}), resulting in 5704 events, overshadowing our 700 events from GF in

N mass	Region	GF	VBF
15 GeV	SR	700	74
	CR2	329	28
	CR1	494	130
	Bkg	1276	98
50 GeV	SR	55	20
	CR2	43	12
	CR1	131	29
	Bkg	43	19

Table 6: Number of events for GF and VBF processes after cuts and corrections for real number of events.

the SR.

The decomposition of this result is seen in Fig. 8, 9, 10 and 11, where we show the event distribution for t_γ bins within the $|\Delta z_\gamma|$ categories. It is clear which t_γ and $|\Delta z_\gamma|$ bins contain the most signal. For the purpose of this thesis, we will focus only on the signal region and refer to the background region as the aggregate of CR1, CR2 and Bkg regions. We see that for all scenarios, there are events for at most the first two bins in t_γ. Also in the $m_N = 50$ GeV scenario, both for GF and VBF, we get more $|\Delta z_\gamma|$ bins with a higher number of events per bin in the signal region compared to the background region, showing that in general our analysis is more sensitive to $|\Delta z_\gamma|$ rather than t_γ.
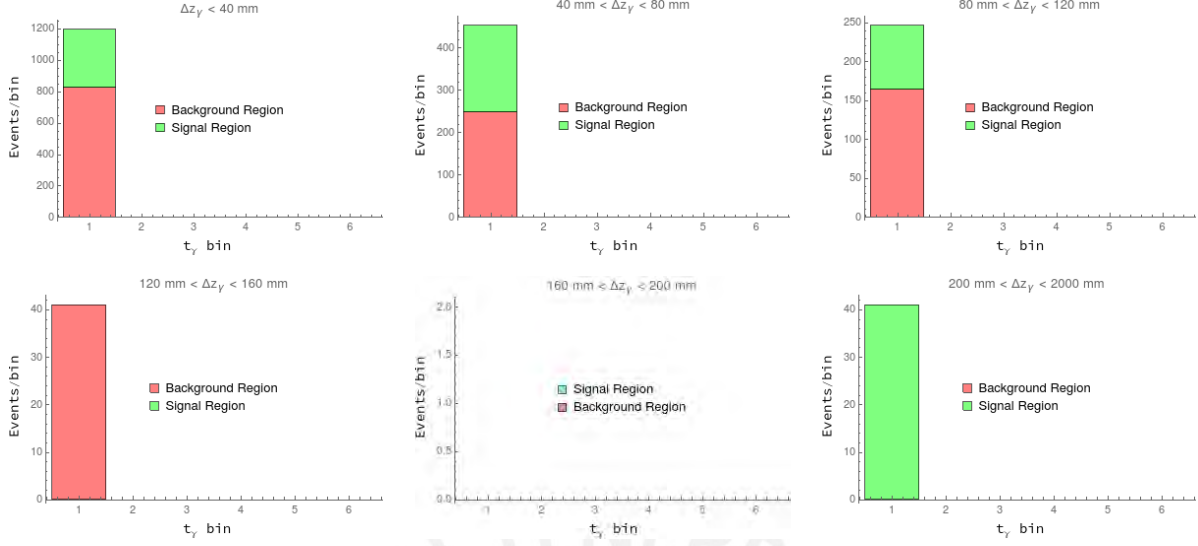
Figure 8: Signal and background regions for the six $|\Delta z_\gamma|$ categories from Table 5 for GF events with $m_N = 15$ GeV.
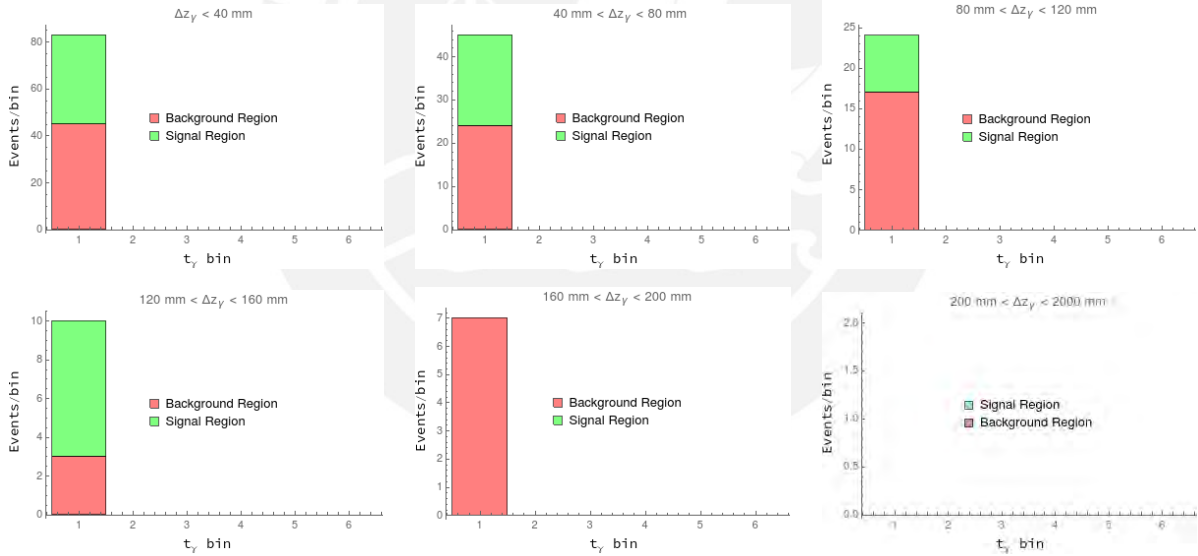

Figure 9: Signal and background regions for the six $|\Delta z_\gamma|$ categories from Table 5 for VBF events with $m_N = 15$ GeV.
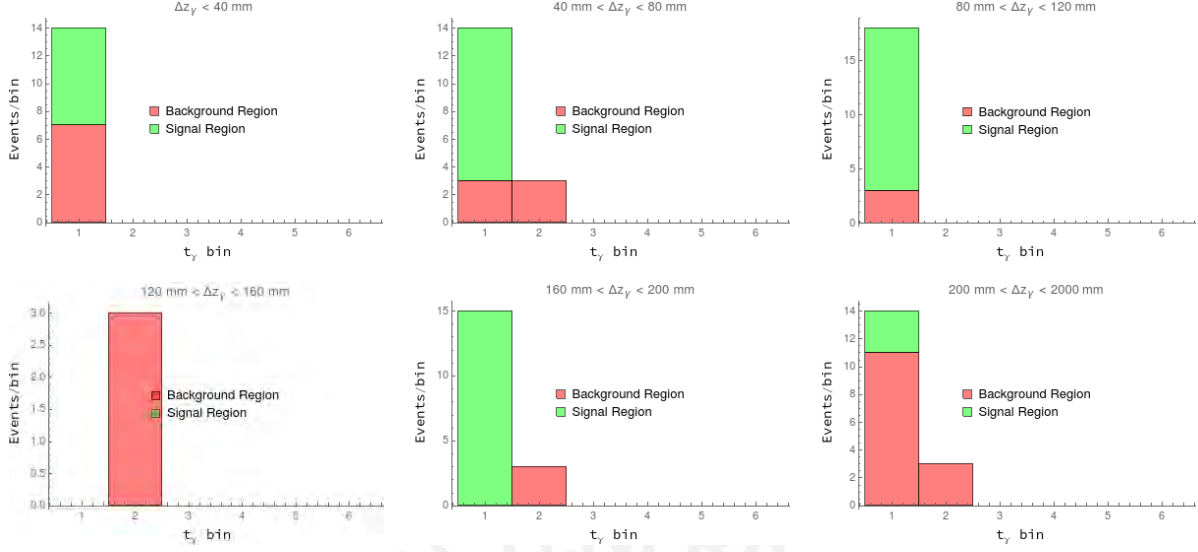
Figure 10: Signal and background regions for the six $|\Delta z_\gamma|$ categories from Table 5 for GF events with $m_N = 50$ GeV.
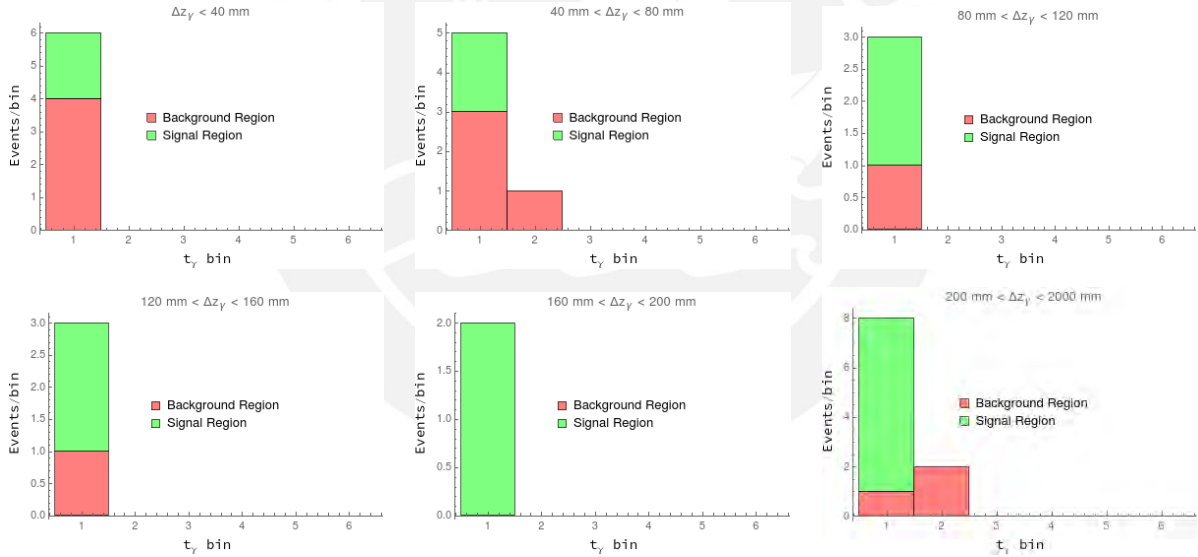

Figure 11: Signal and background regions for the six $|\Delta z_\gamma|$ categories from Table 5 for VBF events with $m_N = 50$ GeV.

Despite having few events, if they were concentrated in regions of high values for $|\Delta z_\gamma|$ and t_γ we might consider a signal differentiated from the background, since the background is highly dominated by

small values for $|\Delta z_\gamma|$ and t_γ. As seen in Fig. 8, 9, 10 and 11, this is not the case.

4 Conclusion

In this work we analyzed heavy neutrinos from GF and VBF processes in the regime where they are long-lived to study their possible detection in the LHC using non-pointing photon searches. We considered a 3+3 Seesaw Type I model where we introduced two right-handed nearly-degenerate neutrinos with masses in the GeV scale and a third neutrino with mass 1 MeV and negligible mixing to the other states, thus behaving like a 3+2 effective model. We analyzed a first scenario where the degenerate masses are ~ 15 GeV and a second one where they are ~ 50 GeV. We provided an enhancement to the mixing by considering large values for γ_{ij} and selected the appropriate mixing values to allow for long-lived particle behaviour.

Proton-proton collision were simulated in MadGraph with collision energy of 13 TeV, obtaining leading order cross-sections of $\sim$

17 and 3 pb for GF and VBF processes respectively. Using both displacement and time-delay variables ($|\triangle z_\gamma|$ and t_γ) and considering a luminosity of $300\,fb^{-1}$ at the LHC, we found that for long-lived heavy neutrinos there is almost 10 times more anticipated number of events at the LHC through GF compared to VBF, with 700 (15) events in the signal region for $M_N = 15(50)GeV$ through GF. The number of events in the control and background regions are comparable to the signal region events, implying that our model significantly contaminates the former. Furthermore, we estimate having 6000 background events in the signal region, contaminating our signal. It is thus not reasonable to expect that, when adding real backgrounds, it will be possible to confidently confirm signal events as such. We also noticed that the after-cuts events are restricted to small values for t_γ but well distributed along $|\triangle z_\gamma|$, suggesting the analysis is more sensitive to the latter parameter.

A Implementation in SPheno and MG5

In order to implement our model for further use in `MadGraph` we used `SARAH`, a `Mathematica` package used to extract Feynman rules from new physics lagrangians. Using version 4.14.2, all the model information was written in a UFO format, a `MadGraph` friendly structure which was later used as input in `MadGraph` 2.6.6 as the model to be used.

The param cards used in `MadGraph` were generated through `SPheno` 4.0.3. `SPheno` (Supersymmetric Phenomenology) is a Fortran based program capable of calculating the particle spectrum for the models implemented in `SARAH`, as well as determining their 2- and 3-body decay widths. We modified `SPheno` by adding the heavy neutrino's 2-body decay partial width, as shown in Eq. 50, to the code already containing the 3-body decays. We also added a subroutine in the input/output script to read the 9 inputs from our effective coupling and later print them as a block with the adequate format in the param card. Using `Mathematica` to input our model's parameters, we then

called SPheno to generate the desired param card.

These param cards were later used in MadGraph after generating our process. This involved loading the UFO file and later launching the process for 10000 unweighted events and 2 proton beams with 6.5 TeV each as to simulate proton-proton collisions at the LHC.

B   HepMC data extraction and processing

HepMC [26] is a C++ based object oriented event record for Monte Carlo Generators and simulation used in High Energy Physics. After running MadGraph and Pythia, HepMC outputs event information after collision for the desired interaction process including all decay products and hadronization in a vertex to outgoing-particles order. All the information, including vertex position, number of outgoing particles, particle 4-momentum, mass and more, at truth level.

We first assumed a cylindrical shape for the ATLAS detector, with a radius of 1.4m and length of 3m up to the electromagnetic calorimeters and used HepMC data to find the point of decay of the desired

heavy neutrinos, as well as their momentum in the interaction. Information from the heavy neutrino decay products (photon and light neutrino) was also registered, in order to extract their pseudorapidity within the EM calorimeters. This allowed us to calculate the photon's time of flight, the heavy neutrino's decay length (whether it is prompt or not and where it decays) and the photon's projected origin in the beamline axis.

C $\triangle z_\gamma$ calculation: closest point between two skew lines

Let us consider two lines in 3-dimensions, L_1 and L_2, represented by vectors $\bar{b}_1$ and $\bar{b}_2$ respectively and 2 points in those lines represented by the vectors $\bar{a}_1$ and $\bar{a}_2$

$$L_1 : \bar{v}_1 = \bar{a}_1 + t_1\bar{b}_1$$
$$L_2 : \bar{v}_2 = \bar{a}_2 + t_2\bar{b}_2 \tag{53}$$

Then the point in L_1 closest to L_2 is:

$$\bar{c}_1 = \bar{a}_1 + \frac{(\bar{a}_2 - \bar{a}_1) \cdot \bar{n}_2}{\bar{b}_1 \cdot \bar{n}_2} \bar{b}_1 \tag{54}$$

with

$$\bar{n}_2 = \bar{b}_2 \times (\bar{b}_1 \times \bar{b}_2) \tag{55}$$

We want to find Δz_γ, the separation along the detector's z-axis (beamline direction) between the event's primary vertex z_{PV} and the projected origin of the photon. To find the projected origin of the photon in the z-axis $z_{\gamma O}$ we consider two lines represented by the following vectors:

$$
\begin{aligned}
L_1 &: \bar{z} = \bar{0} + t_1 \hat{z} \\
L_2 &: \bar{r}_\gamma = \bar{r}_0 + t_2 \frac{\bar{p}}{|\bar{p}|}
\end{aligned}
\tag{56}
$$

Here, $\bar{z}$ represents the z-axis, with $\hat{z} = (0, 0, 1)$ and $\bar{r}_\gamma$ the photon's trajectory, with $\bar{r}_0 = (x_0, y_0, z_0)$ its production origin and $\bar{p}$ its momentum. Then, using Eq. 55 we find $\bar{n}_2$

$$\bar{n}_2 = \frac{\bar{p}}{|\bar{p}|} \times (\hat{z} \times \frac{\bar{p}}{|\bar{p}|}) = \frac{(-p_x p_z, -p_y p_z, p_x^2 + p_y^2)}{|\bar{p}|^2} \tag{57}$$

and introduce this result together with Eq. 56 in Eq. 54 to find the point in the z-axis closest to the photon's trajectory.

$$\bar{c}_1 = \bar{0} + \frac{(\bar{r}_0 - \bar{0}) \cdot \bar{n}_2}{\hat{z} \cdot \bar{n}_2} \hat{z} = \frac{(x_0, y_0, z_0) \cdot (-p_x p_z, -p_y p_z, p_x^2 + p_y^2)}{p_x^2 + p_y^2} (0, 0, 1)$$

$$(58)$$

Then the position in the beamline axis, closest to the photon's trajectory is

$$|\bar{c}_1| = \left| \frac{-p_x p_z x_0 - p_y p_z y_0 + z_0 (p_x^2 + p_y^2)}{p_x^2 + p_y^2} \right|$$
$$= \left| \frac{-p_z (p_x x_0 + p_y y_0 + p_z z_0) + z_0 (p_x^2 + p_y^2 + p_z^2)}{p_x^2 + p_y^2 + p_z^2 - p_z^2} \right| \qquad (59)$$
$$= \left| \frac{z_0 - p_z (\bar{p} \cdot \bar{r}_0) / |\bar{p}|^2}{1 - p_z^2 / |\bar{p}|^2} \right|$$

Thus, finally

$$|\Delta z_\gamma| = ||\bar{c}_1| - z_{PV}| = \left| \frac{z_0 - p_z (\bar{p} \cdot \bar{r}_0) / |\bar{p}|^2}{1 - p_z^2 / |\bar{p}|^2} - z_{PV} \right| \qquad (60)$$

References

[1]   Y. Fukuda et al. "Evidence for Oscillation of Atmospheric Neutrinos". In: *Phys. Rev. Lett.* 81 (8 1998), pp. 1562–1567. DOI: `10.1103/PhysRevLett.81.1562`. URL: `https://link.aps.org/doi/10.1103/PhysRevLett.81.1562`.

[2]   M. Aker et al. "Direct neutrino-mass measurement with sub-electronvolt sensitivity". In: *Nature Phys.* 18.2 (2022), pp. 160–166. DOI: `10.1038/s41567-021-01463-1`. arXiv: `2105.08533 [hep-ex]`.

[3]   Murray Gell-Mann, Pierre Ramond, and Richard Slansky. *Complex Spinors and Unified Theories*. 2013. arXiv: `1306.4669 [hep-th]`.

[4]   Rabindra N. Mohapatra. "Neutrino Mass and Spontaneous Parity Nonconservation". In: *Phys. Rev. Lett.* 44 (14 1980), pp. 912–915. DOI: `10.1103/PhysRevLett.44.912`. URL: `https://link.aps.org/doi/10.1103/PhysRevLett.44.912`.

[5]   Tsutomu Yanagida. "Horizontal gauge symmetry and masses of neutrinos". In: *Conf. Proc. C* 7902131 (14 1979). Ed. by Osamu Sawada and Akio Sugamoto, pp. 95–99. DOI: `10.1103/PhysRevLett.44.912`. URL: `https://link.aps.org/doi/10.1103/PhysRevLett.44.912`.

[6]   Peter Minkowski. "$\mu \to e\gamma$ at a rate of one out of 109 muon decays?" In: *Physics Letters B* 67 (14 Apr. 1977), pp. 421–428. DOI: `10.1016/0370-2693(77)90435-X`. URL: `https://link.aps.org/doi/10.1103/PhysRevLett.44.912`.

[7]   Frank F Deppisch, P S Bhupal Dev, and Apostolos Pilaftsis. "Neutrinos and collider physics". In: *New Journal of Physics* 17.7 (14 2015), p. 075019. DOI: `10.1088/1367-2630/17/7/075019`. URL: `https://doi.org/10.1088%2F1367-2630%2F17%2F7%2F075019`.

[8]   Asli M. Abdullahi et al. "The Present and Future Status of Heavy Neutral Leptons". In: *2022 Snowmass Summer Study*. Vol. 44. American Physical Society, Mar. 2022, pp. 912–

915. DOI: `10.1103/PhysRevLett.44.912`. arXiv: `2203.08039 [hep-ph]`. URL: `https://link.aps.org/doi/10.1103/PhysRevLett.44.912`.

[9] Alberto M. Gago et al. "Probing the Type I Seesaw Mechanism with Displaced Vertices at the LHC". In: *Eur. Phys. J.* C75.10 (14 2015), p. 470. DOI: `10.1140/epjc/s10052-015-3693-1`. arXiv: `1505.05880 [hep-ph]`. URL: `https://link.aps.org/doi/10.1103/PhysRevLett.44.912`.

[10] J. Jones-Pérez, J. Masias, and J. D. Ruiz-Álvarez. "Search for long-lived heavy neutrinos at the LHC with a VBF trigger". In: *The European Physical Journal C* 80.7 (14 2020), pp. 912–915. ISSN: 1434-6052. DOI: `10.1140/epjc/s10052-020-8188-z`. URL: `http://dx.doi.org/10.1140/epjc/s10052-020-8188-z`.

[11] J.A. Casas and A. Ibarra. "Oscillating neutrinos and →e,". In: *Nuclear Physics B* 618.1-2 (14 2001), pp. 171–204. DOI: `10.1016/s0550-3213(01)00475-8`. URL: `https://doi.org/10.1016%2Fs0550-3213%2801%2900475-8`.

[12] A. Donini et al. "The minimal 3+2 neutrino model versus oscillation anomalies". In: *JHEP* 07 (14 2012), p. 161. DOI: `10.1007/JHEP07(2012)161`. arXiv: `1205.5230 [hep-ph]`. URL: `https://link.aps.org/doi/10.1103/PhysRevLett.44.912`.

[13] F. Staub. *Sarah*. 2012. DOI: `10.1103/PhysRevLett.44.912`. arXiv: `0806.0538 [hep-ph]`. URL: `https://link.aps.org/doi/10.1103/PhysRevLett.44.912`.

[14] W. Porod. "SPheno, a program for calculating supersymmetric spectra, SUSY particle decays and SUSY particle production at e+ e- colliders". In: *Comput. Phys. Commun.* 153 (14 2003), pp. 275–315. DOI: `10.1016/S0010-4655(03)00222-4`. arXiv: `hep-ph/0301101 [hep-ph]`. URL: `https://link.aps.org/doi/10.1103/PhysRevLett.44.912`.

[15] W. Porod and F. Staub. "SPheno 3.1: extensions including flavour, CP-phases and models beyond the MSSM". In: *Comput. Phys. Commun.* 183 (14 2011), pp. 2458–2469. DOI: `10.1016/j.cpc.2012.05.021`. arXiv: `1104.1573 [hep-ph]`. URL: `https://link.aps.org/doi/10.1103/PhysRevLett.44.912`.

[16]   Michael L. Graesser. "Broadening the Higgs boson with right-handed neutrinos and a higher dimension operator at the electroweak scale". In: *Phys. Rev. D* 76 (7 2007), p. 075006. DOI: 10.1103/PhysRevD.76.075006. URL: https://link.aps.org/doi/10.1103/PhysRevD.76.075006.

[17]   Michael L. Graesser. *Experimental Constraints on Higgs Boson Decays to TeV-scale Right-Handed Neutrinos*. 2007. DOI: 10.1103/PhysRevLett.44.912. arXiv: 0705.2190 [hep-ph]. URL: https://link.aps.org/doi/10.1103/PhysRevLett.44.912.

[18]   Alberto Aparici et al. "Right-handed neutrino magnetic moments". In: *Phys. Rev. D* 80 (1 2009), p. 013010. DOI: 10.1103/PhysRevD.80.013010. URL: https://link.aps.org/doi/10.1103/PhysRevD.80.013010.

[19]   Gabriel Magill et al. "Dipole portal to heavy neutral leptons". In: *Physical Review D* 98.11 (14 2018), pp. 912–915. ISSN: 2470-0029. DOI: 10.1103/physrevd.98.115015. URL: http://dx.doi.org/10.1103/PhysRevD.98.115015.

[20]   G. Aad et al. "Combined measurements of Higgs boson production and decay using up to 80 fb^{-1} of proton-proton collision data at $\sqrt{s} = 13$ TeV collected with the ATLAS experiment". In: *Phys. Rev. D* 101 (1 2020), p. 012002. DOI: 10.1103/PhysRevD.101.012002. URL: https://link.aps.org/doi/10.1103/PhysRevD.101.012002.

[21]   A. M. Sirunyan et al. "Combined measurements of Higgs boson couplings in proton–proton collisions at $$\sqrt{s}=13\, \text {Te}\text {V} $$". In: *The European Physical Journal C* 79.5 (14 2019), pp. 912–915. DOI: 10.1140/epjc/s10052-019-6909-y. URL: https://doi.org/10.1140%2Fepjc%2Fs10052-019-6909-y.

[22]   F. Delgado et al. *Assessment of the Dimension-5 Seesaw Portal and Impact on Non-Pointing Photon Searches from Exotic Higgs Decays*. 2022. DOI: 10.48550/ARXIV.2205.13550. URL: https://arxiv.org/abs/2205.13550.

[23]   M. Cepeda et al. "Report from Working Group 2: Higgs Physics at the HL-LHC and HE-LHC". In: *CERN Yellow Rep. Monogr.* 7 (14 2019). Ed. by Andrea Dainese et al., pp. 221–

584. DOI: 10.23731/CYRM-2019-007.221. arXiv: 1902.00134 [hep-ph]. URL: https://link.aps.org/doi/10.1103/PhysRevLett.44.912.

[24]   G. Aad et al. "Search for nonpointing and delayed photons in the diphoton and missing transverse momentum final state in 8 TeVppcollisions at the LHC using the ATLAS detector". In: *Physical Review D* 90.11 (14 2014), pp. 912–915. ISSN: 1550-2368. DOI: 10.1103/physrevd.90.112005. URL: http://dx.doi.org/10.1103/PhysRevD.90.112005.

[25]   Abdelhak Djouadi. "The anatomy of electroweak symmetry breaking". In: *Physics Reports* 457.1-4 (14 2008), pp. 1–216. ISSN: 0370-1573. DOI: 10.1016/j.physrep.2007.10.004. URL: http://dx.doi.org/10.1016/j.physrep.2007.10.004.

[26]   Matt Dobbs and Jørgen Beck Hansen. "The HepMC C++ Monte Carlo event record for High Energy Physics☐☐Available via the following web-address: http://home.cern.ch/mdobbs/HepMC/." In: *Computer Physics Communications* 134.1 (14 2001), pp. 41–46. ISSN: 0010-4655. DOI: https://doi.org/10.1016/S0010-4655(00)00189-2. URL: https://www.sciencedirect.com/science/article/pii/S0010465500001892.